

Shortest Secure Path in a Voronoi Diagram

Sariel Har-Peled*

Rajgopal Varadharajan

August 2019

Abstract

We investigate the problem of computing the shortest secure path in a Voronoi diagram. Here, a path is secure if it is a sequence of touching Voronoi cells, where each Voronoi cell in the path has a uniform cost of being secured. Importantly, we allow inserting new sites, which in some cases leads to significantly shorter paths. We present an $O(n \log n)$ time algorithm for solving this problem in the plane, which uses a dynamic additive weighted Voronoi diagram to compute this path. The algorithm is an interesting combination of the continuous and discrete Dijkstra algorithms. We also implemented the algorithm using CGAL.

1. Introduction

Motivation. Consider a facility in an environment where other facilities exist. A client can communicate safely only with its nearest facility. The region where one can safely communicate with the facility, is the *Voronoi cell* of this facility. Given two facilities s and t , consider the problem of creating a safe corridor, where one can safely move from s and t while still being able to communicate safely with both of them. This might require inserting new middle facilities, such that the union of the new Voronoi cells (together with the Voronoi cells of s and t), form a connected set. The natural question is where and how many sites one needs to use/insert to establish such a reliable connection, see [Figure 1.1](#).

Formal problem statement. Let P be a set of n points in the plane, and let $\mathcal{V}(P)$ denote its Voronoi diagram. Two points s, t in the plane can directly communicate *safely*, if s and t are “close” to each other. Formally, we require that the cells of s and t are adjacent in the Voronoi diagram of $P \cup \{s, t\}$ – geometrically, this corresponds to the existence of a disk that contains s and t , and no other points of P . Naturally, most points can not communicate safely. To overcome this, one can insert a set of points $Q = \{q_1, \dots, q_\nu\}$ into the P , such that $q_0 = s$, $q_\nu = t$, and in the new diagram $\mathcal{V}(P \cup Q)$ the point q_i can safely communicate with q_{i+1} , for all i . It is natural to ask for the minimum size set Q , such that s and t can communicate safely, via $\nu - 1$ hops. Note, that a site q_i might be an existing site – this can be interpreted as securing this site (this cost the same as inserting a new site).

A naive approach is to insert s and t into the initial Voronoi diagram, and compute the shortest path between them in the resulting dual graph (i.e., the Delaunay triangulation of $P \cup \{s, t\}$) –

*Department of Computer Science; University of Illinois; 201 N. Goodwin Avenue; Urbana, IL, 61801, USA; sariel@illinois.edu; <http://sarielhp.org/>. Work on this paper was partially supported by a NSF AF award CCF-1907400.

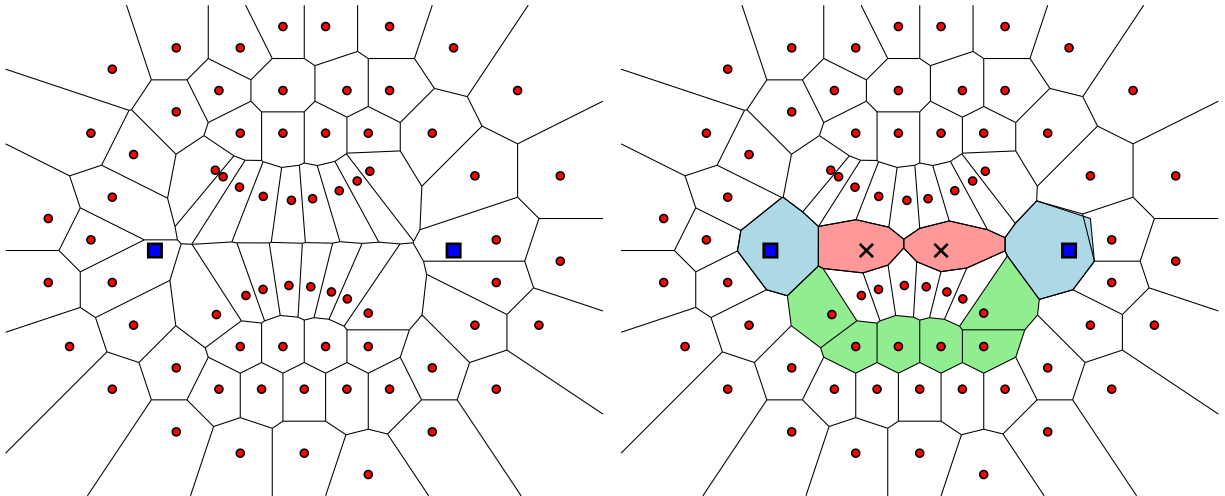


Figure 1.1: Inserting two middle sites is enough. Here we insert both the two endpoints into the diagram, and two middle sites (i.e., the two red cells). Note, that one can secure an existing site, instead of inserting a new one – this has the same cost. In this specific example, if one uses only existing cells, the price is six (the green cells).

this corresponds to adding all the intermediate nodes in this path to Q . However, there are natural scenarios, see [Figure 1.1](#), where allowing the sites to be placed arbitrarily in the plane significantly reduces the number of sites needed. As mentioned earlier, the price of securing an existing site, or introducing a new site is the same.

Our results. We describe how the region of reachable points after t insertions look like, and show to compute it efficiently. We then describe an $O(n \log n)$ time algorithm for computing the shortest such path between two points, using a process that is a variant of the Dijkstra algorithm. We implemented the algorithm using CGAL, and provide the source code.

Related results. The basic algorithm is a variant of continuous Dijkstra, a technique that was used for shortest path algorithms among obstacles, and for shortest path on polyhedral surfaces in three dimensions [\[MMP87\]](#). The basic process of inserting points, is similar in nature to Delaunay refinement [\[Rup95\]](#). The new algorithm can be viewed as a combination of these two techniques.

2. The algorithm

Notations. For a point p and a radius r , let $\bullet(p, r)$ denotes the disk of radius r centered at p . For a set of objects \mathcal{X} , in the plane, let $\mathcal{V}(\mathcal{X})$ denote the Voronoi diagram of \mathcal{X} . For an object x , let $\text{cell}_x(\mathcal{X})$ denote the cell of x in the Voronoi diagram of $\{x\} \cup \mathcal{X}$.

2.1. Understanding the problem: The flowering process

As an example, consider a point set formed by a hexagonal lattice – see [Figure 2.1](#). Let $q_0 = s$ be a starting site (which is one of the points of the lattice), and assume our purpose is to reach a site

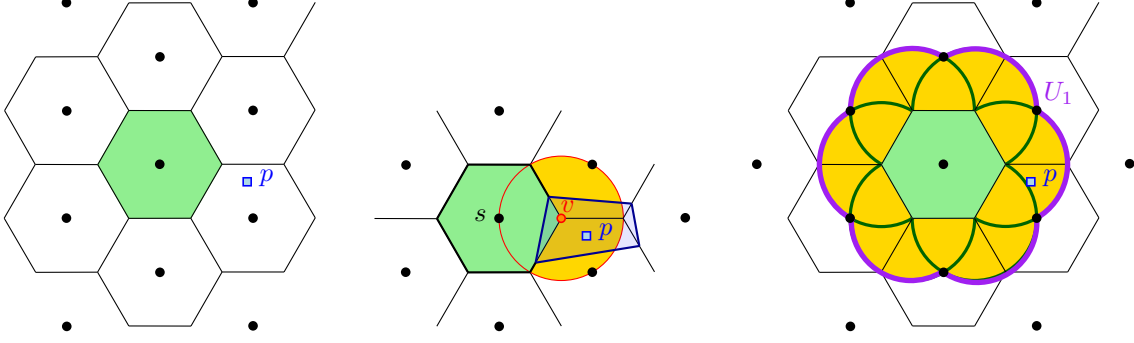


Figure 2.1: The hexagonal case.

$q_\nu = t \in P$. The site s can communicate directly with all the sites that are adjacent to its Voronoi cell $R_0 = \text{cell}_s(P)$, without requiring the insertion of any middle sites.

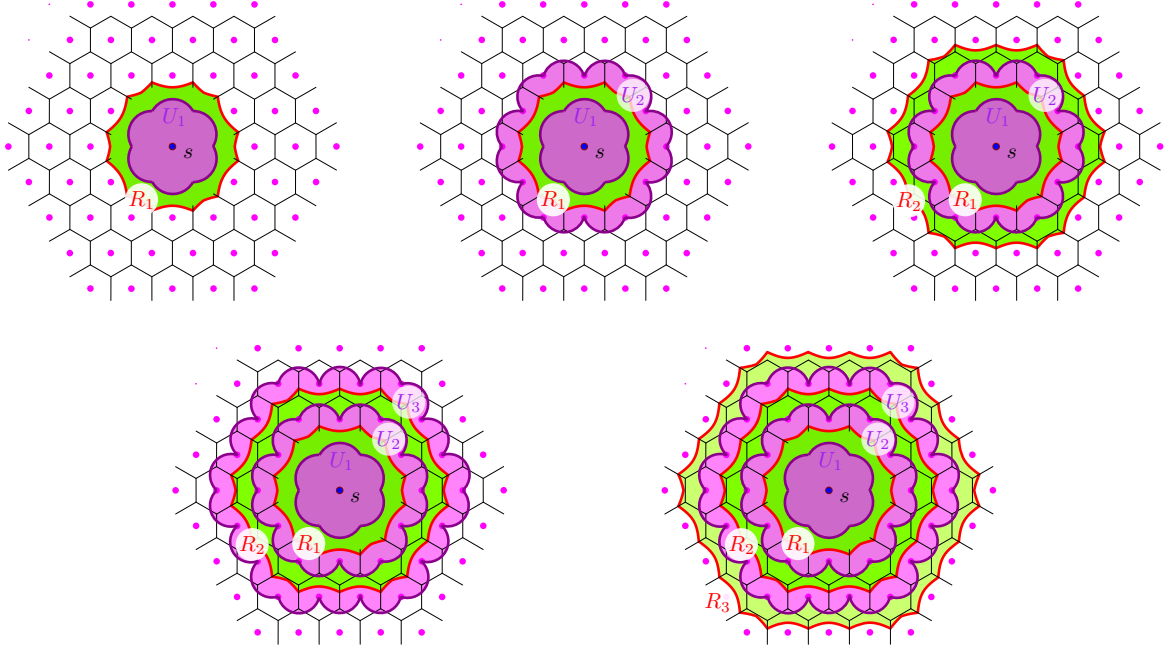


Figure 2.2: The flowering process of how the shortest path region grows.

If we insert a new middle site q_1 , then its cell must touch the cell of R_0 . Consider such a location p for a middle site. For the new site of p to be adjacent to R_0 , after p is inserted, there must be a point $v \in R_0$, such that v is as close (or closer) to p than it is to $q_0 = s$. This region of influence, where v can be “occupied”, is exactly the disk $\bullet(v, \|v - s\|)$. See Figure 2.1. As such, the allowable region to insert this first site, is

$$U_1 = \cup_{v \in R_0} \bullet(v, \|v - s\|).$$

(Namely, sites inserted outside U_1 are not going to be adjacent to R_0 in the new Voronoi diagram.)

The set U_1 is a union of disks – in this specific case, it is equal to the union of disks placed at vertices of the original Voronoi cell, see [Figure 2.1](#). Indeed, disks centered in the interior of R_0 are covered by disks centered at the boundary of the Voronoi cell. Importantly, the union of disks centered at a Voronoi edge form a pencil which is covered by the two disks induced by the two Voronoi vertices of the edge, see [Figure 2.3](#).

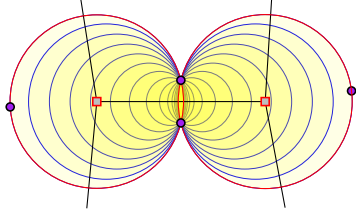


Figure 2.3: A pencil of disks. The union of the two extreme disks of the pencil (i.e., the one induced by the Voronoi vertices), cover the union of the disks in the pencil.

Let $P_1 = P \setminus U_1$. The region that can potentially be covered by such a single insertion of a site into U_1 , belong to the region

$$R_1 = \bigcup_{p \in U_1} \text{cell}_p(P_1),$$

The set R_1 contains all the points, in the plane, that are closer to U_1 , than to any point in P_1 . Namely, $R_1 = \text{cell}_{U_1}(P_1)$. Any site $u \in P_1$ that its Voronoi cell is adjacent to R_1 in $\mathcal{V}(\{U_1\} \cup P_1)$, can communicate with q_0 via the insertion of a single site.

As such, we may treat U_1 simply as the union of disks at the finitely many vertices of R_0 . The boundary of U_1 is all that is necessary to accurately compute the boundary of R_1 (which may be viewed as a wavefront computed by the algorithm). The set R_1 is then the union of Voronoi cells in a Voronoi diagram of disks and points. This underlying diagram is therefore an additive weighted Voronoi diagram, and its boundary edges are portions of hyperbolas and straight segments. See [Figure 2.2](#).

Formally, let the set R_i be the set reachable by inserting i middle sites starting at s . The set U_{i+1} is the region where one can insert an $(i+1)$ th point, q_{i+1} , such that one can form a connected, safe chain back to s . By the discussion above, U_{i+1} can be treated as the union of finitely many disks at the vertices of R_i , with some additional care. Let $P_{i+1} = P \setminus U_i$. The $(i+1)$ th *occupied* region is

$$U_{i+1} = \bigcup_{v \in R_i} \bullet(v, d(v, P \setminus R_i)), \quad (2.1)$$

where $d(v, P) = \min_{p \in P} \|v - p\|$. And the $(i+1)$ th *reachable* region is

$$R_{i+1} = \bigcup_{p \in U_{i+1}} \text{cell}_p(P),$$

As soon as the region R_{i+1} shares a boundary with the Voronoi cell of t , one can stop, and reconstruct the safe path.

2.2. The basic algorithm

The input is a set P of n points in the plane, and two point $s, t \in P$. The algorithm initially computes the Voronoi diagram of P , and has a queue \mathcal{Q} of sites, which is initially set to s . A site here is a disk (the initial point is a disk of radius 0, naturally).

The algorithm works in rounds. In each round, it extracts all the sites in the queue, and inserts them into the current additive weighted Voronoi diagram – these are the outer disks, whose outer boundary forms the boundary of U_i in the i th round. Next, the algorithm scans all the inserted sites, and looks at the adjacent Voronoi vertices of their cells. All of the Voronoi vertices that are outside U_i (how to check for this condition we describe below), are inserted into the queue to be handled in the next round.

Once the wavefront reaches t , the processes stops – or alternatively, we compute this diagram till the whole plane is covered, and preprocess the resulting map for point location.

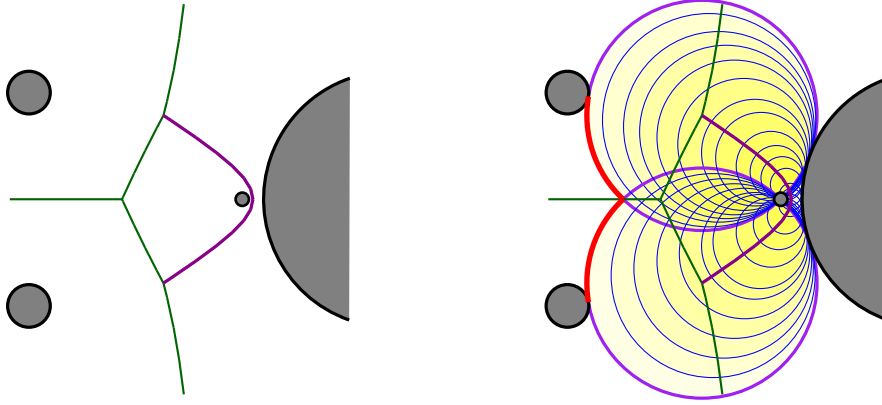


Figure 2.4: The Voronoi diagram of points and disks. A hyperbolic segment in this diagram, and its pencil of disks. Only the two disks, associated with the Voronoi vertices, contribute to the outer boundary of the union of the disks.

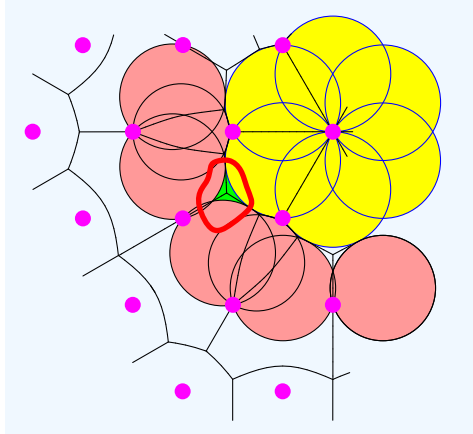


Figure 2.5: Two generations of disks inserted, and a pocket that is left behind. This pocket corresponds to a middle of a hyperbolic edge from previous generation, which was covered by the inserted disks.

What disks to insert. The algorithm inserts the disks of Eq. (2.1). As discussed earlier, one needs to insert only the disks that have their center on the boundary of R_i . This boundary is a union of hyperbolic segments. Each such hyperbolic segment corresponds to a pencil of disks, that are included in the union, but the algorithm inserts only the two extreme disks that corresponds to the vertices of the diagram. See Figure 2.4.

Each such hyperbolic segment of the boundary might give rise to a pocket that is left behind the front. Since these pockets can not contribute to the front, and they are shallow – we leave them behind. Such a pocket is depicted in [Figure 2.5](#).

To correctly leave the pockets behind, the algorithm remembers for each site inserted the layer (i.e., generation) of the propagation it came from. As such, when inspecting a Voronoi vertex, the sites that gave rise to it, and their generation are known. All sites that are from two or more generations ago are not inserted, thus blocking the wavefront from propagating backwards.

Reconstructing the shortest path. The above insertion process creates “rings” of inserted disks, where each generation forms a single ring, see [Figure 3.1](#) for an example. Importantly, every insert disk of a certain generation touches a disk of a previous generation, where a disk of the first generation touches the source vertex. As such, for every such disk there is a chain of touching disks that goes back to the source. This is the *insertion path* of this disk.

As such, when the wavefront arrives to the target cell, then in the resulting Voronoi diagram there is a hyperbolic bisection segment of the Voronoi diagram, that separates the target cell from some newly inserted disks. Please any disk D centered at this hyperbolic curve, that touches the target point t . The disk D touches a disk D' that was just inserted. The disk D together with the insertion path forms a sequence of disks that touch each other, and touch s and t . The key observation is that if we insert the points of tangency between two consecutive disks in this sequence, into the original set of points, in the resulting diagram, the newly inserted Voronoi cells form a connected safe zone, as desired. We note that the choice of points to be inserted is not unique. The process is illustrated in [Figure 2.6](#).

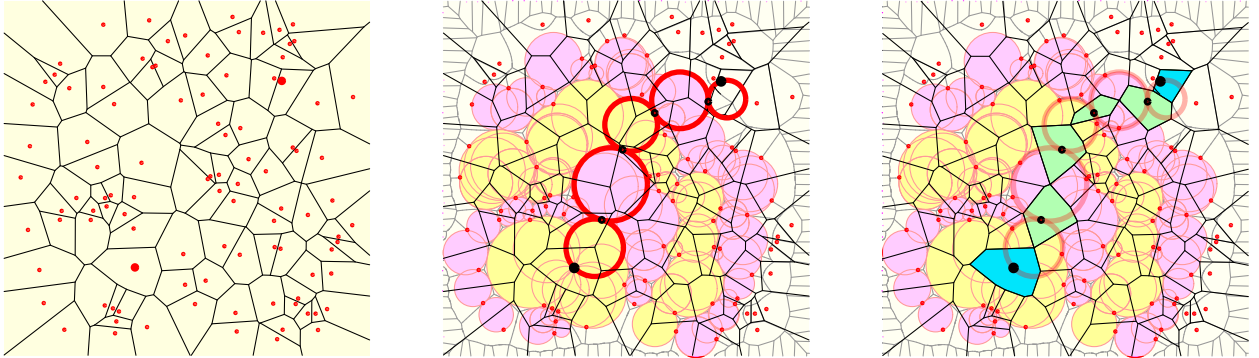


Figure 2.6

2.3. Running time analysis

A point p of the input is *active* at time i , if it is adjacent to a site inserted in the i th iteration.

Lemma 2.1. *An input point can be active for at most two iterations.*

Proof: An input point p is *discovered* at time i , if its Voronoi cell C in $\mathcal{V}_i = \mathcal{V}(\{U_i\} \cup (P \setminus U_i))$ is adjacent to the cell of U_i in this diagram.

Informally, once a cell is being discovered, in the next iteration of insertions, disks would be inserted that touch it, and the following iteration it would be blocked from the (wave) front. Namely, the boundaries of C and R_i intersect, as R_i is the cell of U_i in \mathcal{V}_i . As such, p is on the boundary of

U_{i+1} , or p might be contained in the interior of U_{i+1} . Indeed, consider a point q on the common boundary between C and R_i , and consider the disk of radius $\|p - q\|$ centered at q , and observe that this disk has p on its boundary, and it is contained in U_{i+1} , see [Eq. \(2.1\)](#). But that implies that C is contained in the Voronoi cell of U_{i+1} in $\mathcal{V}_{i+1} = \mathcal{V}(\{U_{i+1}\} \cup (P \setminus U_{i+1}))$. This cell is thus R_{i+1} . Thus, the cell of p might interact with cells created in U_i , and U_{i+1} . Clearly, p can not be adjacent to cells inserted in later iterations. ■

Let n_i be the number of the active input points at time i . Since inserting a disk, updating the Voronoi diagram, and discovering the new Voronoi sites is all done locally, and can be charged to new entities created or deleted, the following is straightforward to verify. It is critical here that we are inserting sites centered at Voronoi vertices, which we already know their location – that is, there is no need to perform point-location query for the insertion. As such, we get the following.

Lemma 2.2. *The total running time of the i th iteration, is bounded by $O(\sum_{j=i-2}^{i+2} n_j)$.*

Proof: We only sketch the proof. The quantity stated above bounds the number of sites that the wavefront might interact with in the i th iteration. In particular, it bounds the number of sites inserted at time i . By [Lemma 2.1](#), a site is active only for a constant number of iterations. A new site inserted which is adjacent only to inserted sites, is a pocket, and the algorithm does not insert it. As such, inserted sites must be adjacent to original input points. It is easy to verify that an input site can support only a constant number of such sites around it, which readily implies that while a site is active, only a constant number of new sites inserted might be charged to it.

This implies by planarity, that the total complexity of the Delaunay triangulation in the i th iteration is proportional the total complexity of the input points in the adjacent layers, which implies the claim. ■

Theorem 2.3. *The running time of the algorithm is $O(n \log n)$.*

Proof: Reading the input and computing the Voronoi diagram takes $O(n \log n)$ time. By [Lemma 2.2](#), the total running time of the later stages is proportional to $\sum_i O(n_i) = O(n)$. ■

3. Implementation and some pictures

The algorithm was implemented in C++ using CGAL [[The20](#)]. Specifically, we use the 2D Apollonius Graphs implementation (which was implemented by Menelaos Karavelas and Mariette Yvinec), see [[Kar20](#), [KY20](#)].

The source is available at bitbucket https://bitbucket.org/vrdhrjn2/voronoi_insertion. The repository also includes an input file, and a script to run the program on various inputs.

[Figure 3.1](#) illustrates the execution of the algorithm on a random input, [Figure 3.2](#) is for a real world input, which is a point set of locations in illinois (downloaded from the census). [Figure 3.3](#) illustrates the execution of the algorithm on a hexagonal grid. [Figure 3.4](#) summarizes the inputs tested, and the execution on them. The point sets that are generated are of three types: diagrams of regular hexagonal Voronoi cells, diagrams of randomly chosen points, and diagrams of points representing the state of Illinois constructed from census data.

Bounding points along the edges of a bounding box of the point set are added for the underlying additive diagram phase of the algorithm, to ensure no edges are infinite. The start and end points

are chosen by considering a rectangular subset of points in the interior and choosing the furthest two points among them. Then the algorithm is run until a path is found safely connecting the two cells.

Potential floating point or degeneracy issues are avoided by adding small perturbations to the point set as points are inserted into the initial diagram. Radii of the disks being inserted in the additive diagram phase are also dilated by a very small factor for the same reasons.

While we are not reporting the running times, they seem to be near linear, and agree with the theoretical analysis (ignoring the initial construction time).

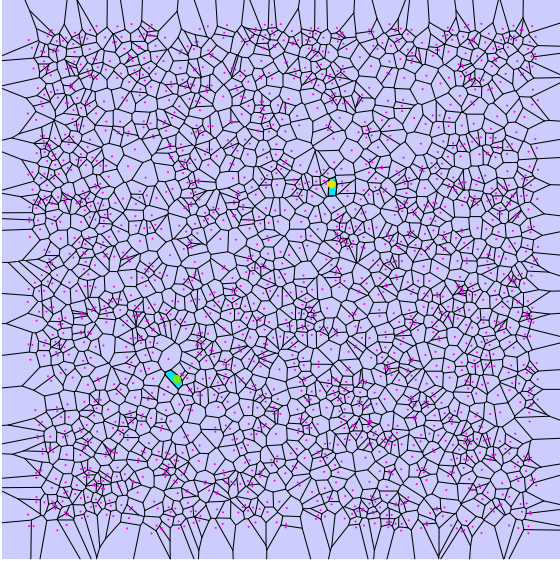
We used the CGAL Apollonius Graph hierarchy for the implementation. The provided library insertion function has two phases - locating a nearest neighbor, and then constructing a new Voronoi cell by identifying conflict edges, etc. The nearest neighbor location in our algorithm can theoretically be done in constant time, because all the points we insert are Voronoi vertices whose adjacent sites are immediately known. However, we did not bypass the internal nearest neighbor search because the results of using the Apollonius Graph hierarchy were already linear time in practice.

On different point sets, the overall run time is not affected by the type of mesh chosen (for the same number of points). However, on regular hex meshes the BFS and algorithm paths have the same length, and small improvements in practice are noticed because of the perturbations we apply and when there are a large number of points. For other point sets, significant improvements are always noticed.

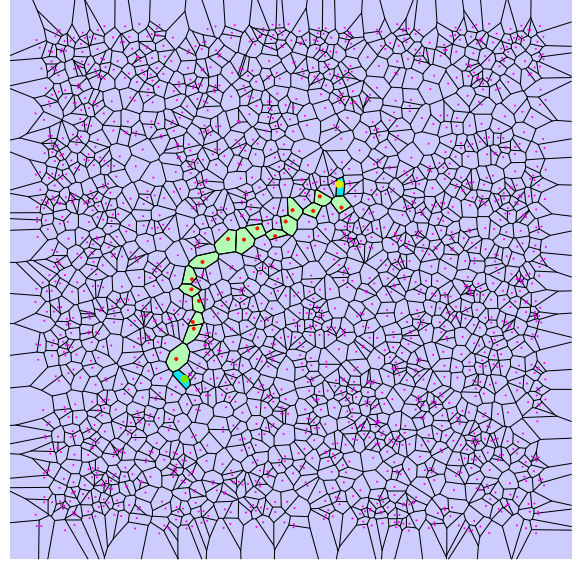
Acknowledgement. The authors would like to thank Alon Efrat – long time ago he mentioned this problem to the first author.

References

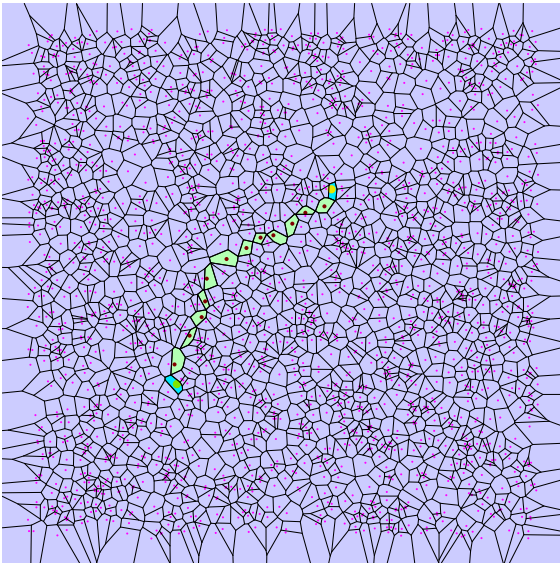
- [Kar20] Menelaos Karavelas. *2D voronoi diagram adaptor*. In *CGAL User and Reference Manual*. CGAL Editorial Board, 5.0.2 edition, 2020.
- [KY20] Menelaos Karavelas and Mariette Yvinec. *2D apollonius graphs (delaunay graphs of disks)*. In *CGAL User and Reference Manual*. CGAL Editorial Board, 5.0.2 edition, 2020.
- [MMP87] J. S.B. Mitchell, D. M. Mount, and C. H. Papadimitriou. The discrete geodesic problem. *SIAM Journal on Computing*, 16(4):647–668, 1987.
- [Rup95] Jim Ruppert. A Delaunay refinement algorithm for quality 2-dimensional mesh generation. *J. Algorithms*, 18(3):548–585, 1995.
- [The20] The CGAL Project. *CGAL User and Reference Manual*. CGAL Editorial Board, 5.0.2 edition, 2020.



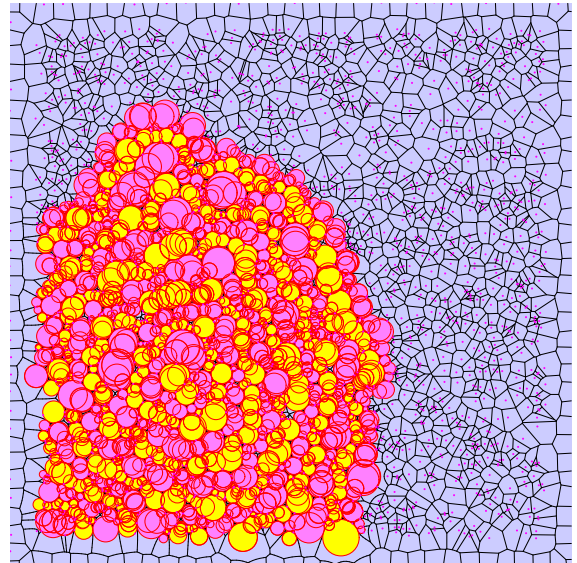
Input



BFS shortest path (16 intermediate points)

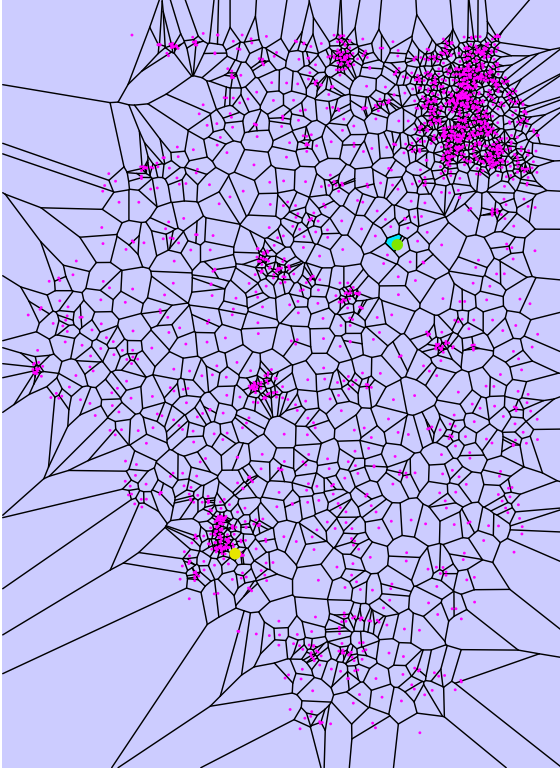


Algorithm shortest path (12 intermediate points)

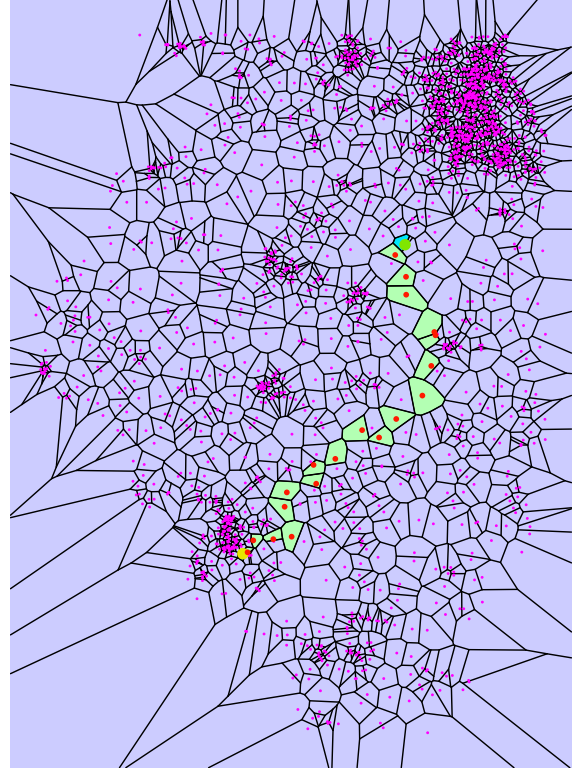


Sites inserted during execution.

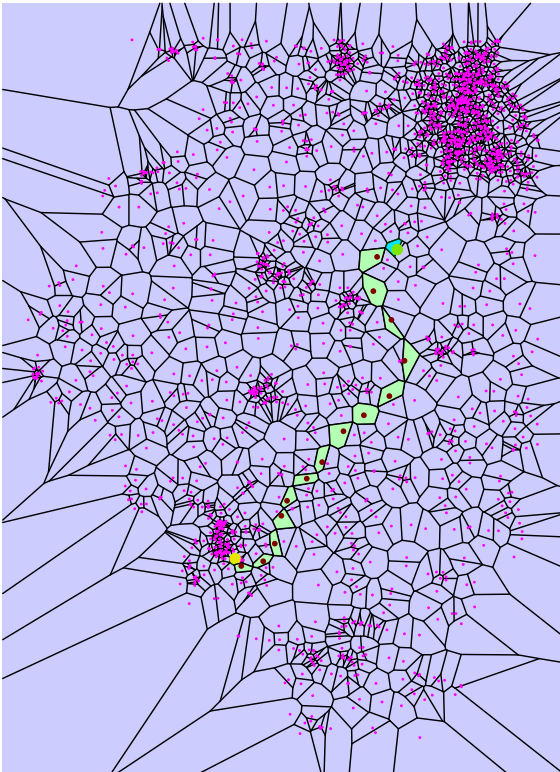
Figure 3.1: A random point set with 2000 points, and the algorithm execution on it.



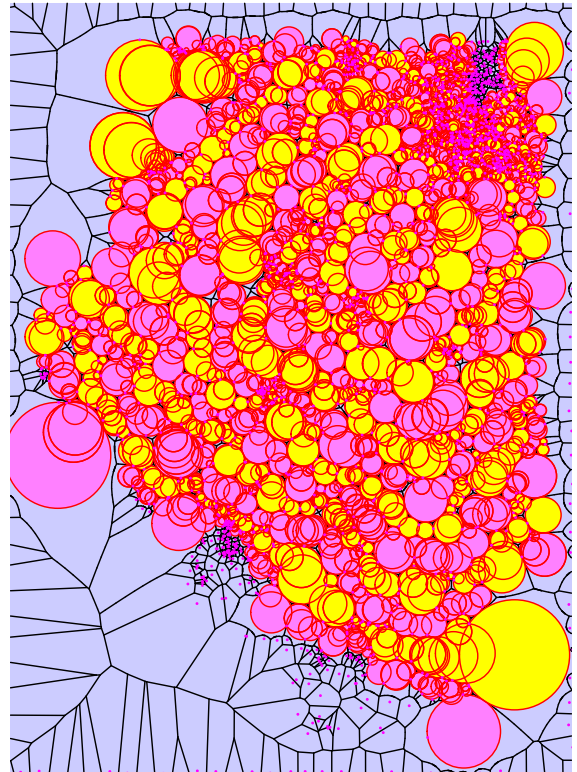
Input



BFS shortest path (19 intermediate points)

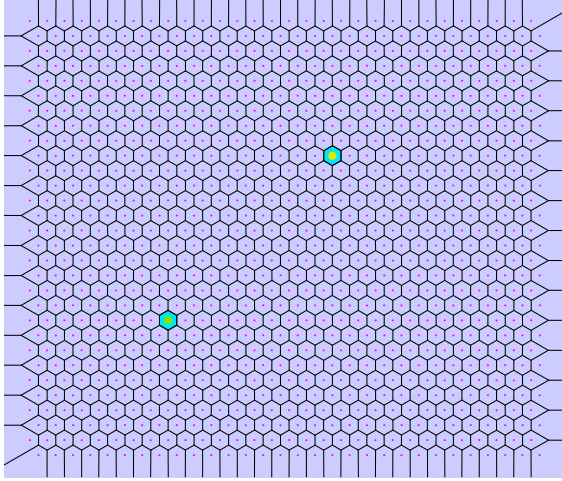


Algorithm shortest path (14 intermediate points)

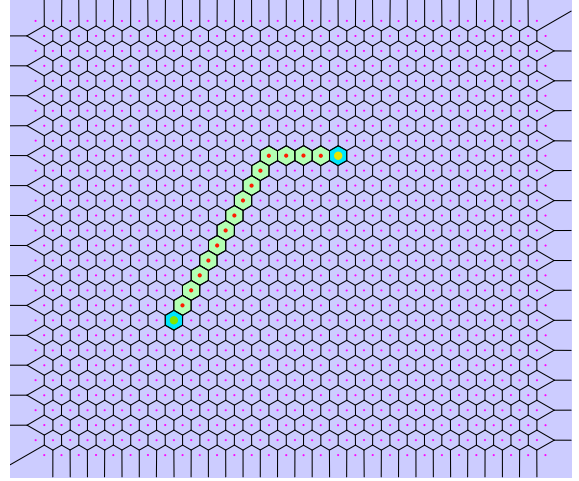


Sites inserted during execution.

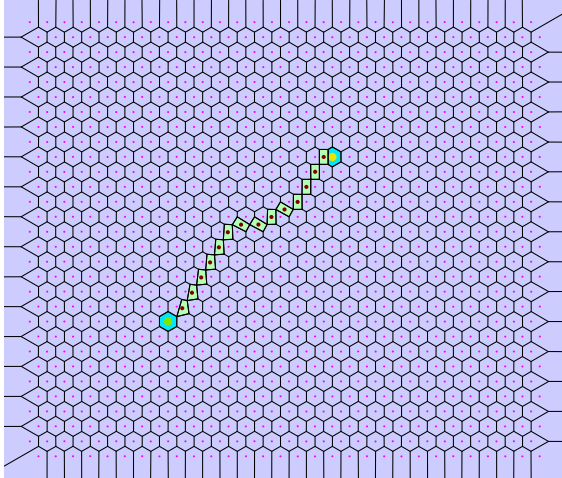
Figure 3.2: A point set made out of locations in Illinois (downloaded from the census and sparsified), and the algorithm execution on it.



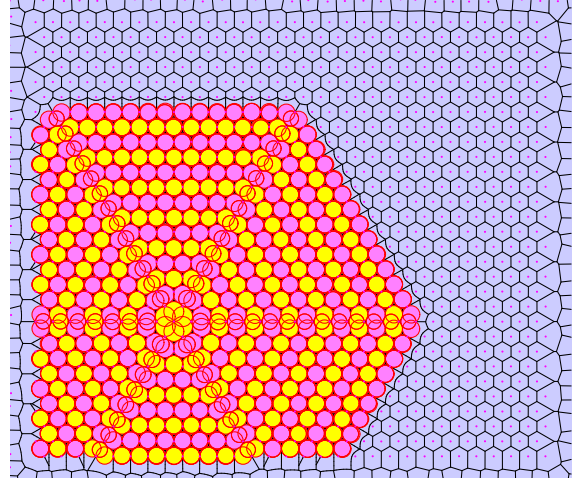
Input



BFS shortest path (14 intermediate points)



Algorithm shortest path (14 intermediate points)



Sites inserted during execution.

Figure 3.3: A point set made out of a hexagonal grid, and the algorithm execution on it.

| Input name | # points | BFS path | Algorithm path len |
|-------------|----------|----------|--------------------|
| hex_010 | 100 | 5 | 5 |
| hex_030 | 900 | 18 | 18 |
| hex_060 | 3,600 | 56 | 54 |
| hex_090 | 8,100 | 63 | 61 |
| hex_120 | 14,400 | 77 | 75 |
| i.d_02 | 17,560 | 55 | 38 |
| i.d_04 | 8,816 | 39 | 28 |
| i.d_08 | 4,435 | 30 | 23 |
| i.d_16 | 2,242 | 22 | 15 |
| i.d_32 | 1,123 | 17 | 12 |
| i.d_64 | 559 | 11 | 9 |
| rand_00100 | 100 | 5 | 4 |
| rand_00200 | 200 | 8 | 6 |
| rand_00400 | 400 | 12 | 9 |
| rand_01000 | 1,000 | 17 | 14 |
| rand_02000 | 2,000 | 28 | 21 |
| rand_04000 | 4,000 | 37 | 30 |
| rand_08000 | 8,000 | 47 | 38 |
| rand_16000 | 16,000 | 76 | 61 |
| rand_32000 | 32,000 | 95 | 74 |
| rand_64000 | 64,000 | 137 | 110 |
| rand_128000 | 128,000 | 206 | 164 |

Figure 3.4: Input used, and the algorithm performance on these inputs.